

A NOVEL APPROACH TO CONSTRAIN THE ESCAPE FRACTION AND DUST CONTENT AT HIGH REDSHIFT USING THE COSMIC INFRARED BACKGROUND FRACTIONAL ANISOTROPY

ELIZABETH R. FERNANDEZ¹, HERVE DOLE¹, ILIAN T. ILIEV²

¹Institut d'Astrophysique Spatiale, Univ Paris-Sud 11 and CNRS, Orsay F-91405, France

²Astronomy Centre, Department of Physics & Astronomy, Pevensey II Building, University of Sussex, Falmer, Brighton BN1 9QH
Draft version March 12, 2018

Abstract

The Cosmic Infrared Background (CIB) provides an opportunity to constrain many properties of the high redshift ($z > 6$) stellar population as a whole. This background, specifically from 1 to 200 microns, should contain information about the era of reionization and the stars that are responsible for these ionizing photons. In this paper, we look at the fractional anisotropy ($\delta I/I$) of this high redshift population, where δI is the ratio of the magnitude of the fluctuations and I is the mean intensity. We show that this can be used to constrain the escape fraction of the population as a whole, because the magnitude of the fluctuations of the CIB depends on the escape fraction, while the mean intensity does not. This results in lower values of the escape fraction producing higher values of the fractional anisotropy. This difference is predicted to be larger at longer wavelengths bands (above 10 microns), albeit it is also much harder to observe in that range. We show that the fractional anisotropy can also be used to separate a dusty from a dust-free population. Finally, we discuss the constraints provided by current observations on the CIB fractional anisotropy.

Subject headings: cosmology: theory — diffuse radiation — galaxies: high-redshift — infrared: galaxies

1. INTRODUCTION

Modern cosmology is now able to constrain details about the era of reionization. Observations show that the reionization of the universe occurred early and was extended in time, with an equivalent of an instantaneous reionization at $z \sim 11$ (Komatsu et al. 2009, 2011). Stars are a likely candidate for being responsible for the majority of reionization because they are efficient producers of ultraviolet photons. Thanks to a wave of modern, sensitive telescopes, we can begin to observe and understand the frontier of reionization, along with these high redshift stellar populations ($z > 6$). For example, we can observe these galaxies directly via high redshift surveys, which can now routinely identify a population of bright galaxies up to a redshift of about $z \sim 8$. However, these surveys can only locate those galaxies that are both above the limiting magnitude and common enough to be present in the survey field. It is now thought (Bouwens et al. 2010; Robertson et al. 2010; Fernandez & Shull 2011) that reionization needed a large population of smaller galaxies below the current detection limits. Because we cannot yet observe these galaxies directly, we can instead look for their cumulative light, which should exist as background radiation. Because reionization is said to have occurred around $z \sim 11$, the photons responsible for reionization should be present in the Cosmic Infrared Background (CIB). The spectral peak of this radiation is around the Lyman- α line, which will be redshifted to 1–4 microns. However, continuum emission will create an extended tail at longer wavelengths.

Here, we discuss the CIB from about 1 to 200 microns. The majority of the CIB will be emission from sources below $z \sim 6$, such as our Galaxy, foreground galaxies, and other sources of infrared light, such as zodiacal light. If these sources can be subtracted away to a high precision,

it is possible that the remainder could be from the era of reionization, and if so, could tell us about the properties of these high redshift stars.

There have been many attempts to theoretically model the high redshift component of the CIB, especially in the near-infrared, from the mean (Santos et al. 2002; Magliocchetti et al. 2003; Salvaterra & Ferrara 2003; Cooray & Yoshida 2004; Madau & Silk 2005; Fernandez & Komatsu 2006), to fluctuations (Kashlinsky et al. 2002, 2004, 2005, 2007c, 2012; Kashlinsky 2005; Magliocchetti et al. 2003; Cooray et al. 2004; Thompson et al. 2007a,b; Fernandez et al. 2010, 2012). In this paper, we examine another way to analyze the CIB, the fractional anisotropy, which is the ratio of the fluctuations to the mean. By looking at the fractional anisotropy, many free parameters are removed and more information about this elusive stellar population can be extracted. Specifically, we discuss using the CIB as a probe for the escape fraction of ionizing photons. Finding the escape fraction is important for understanding reionization and its duration. There have been several attempts to measure the escape fraction through analytical models, simulations, and observations (see Fernandez & Shull (2011) and references within). These papers have shown that the escape fraction appears to vary greatly from galaxy to galaxy. Therefore, instead of trying to measure the escape fraction of an individual galaxy, here we discuss the average escape fraction of all galaxies, which will give more of a global view of reionization. In addition, the fractional anisotropy can reveal information about the dust content of galaxies, which is mostly unknown at high redshifts.

We describe our simulations in section 2 and our models in section 3. In section 4, we discuss our method for finding the mean CIB, the fluctuations of the CIB, and the fractional anisotropy. In section 5, we discuss our

¹Elizabeth.Fernandez@ias.u-psud.fr

results of the fractional anisotropy for various bands. In section 6, we discuss the most recent observations. We conclude in section 7. Throughout this paper, we use the cosmological parameters $(\Omega_m, \Omega_\Lambda, \Omega_b, h) = (0.27, 0.73, 0.044, 0.7)$, consistent with the simulations from Iliev et al. (2012), which are based on the WMAP 5-year results and other available constraints (Komatsu et al. 2009).

2. THE SIMULATIONS

In order to predict the angular power spectrum of the CIB, we used simulations from Iliev et al. (2012), which are N-body simulations combined with radiative transfer, which allow us to see how sources are affected by the reionization process. The high resolution of these simulations (with a minimum mass of $10^8 M_\odot$) allow us to also include Jeans-mass filtering on low mass halos. This effectively allows suppression of star formation within small halos ($10^8 - 10^9 M_\odot$) because of elevated gas temperatures that could be caused by the proximity to other star forming galaxies. These simulations have a box size of either $114h^{-1} Mpc$ (for cases with suppression of small sources) or $37h^{-1} Mpc$ (with no suppression, where $M_{min} = 10^8 M_\odot$, or complete suppression, where $M_{min} = 10^9 M_\odot$). These simulations are summarized in Table 1 (Iliev et al. 2012; Fernandez et al. 2012).

To describe the stellar populations within these halos and their relationship with their environment, we define a parameter f_γ , which describes the number of ionizing photons produced per stellar atom that can escape the galaxy and reionize the intergalactic medium (IGM). f_γ is defined as a product of the star formation efficiency, or the fraction of baryons that are in stars (f_*), the escape fraction (f_{esc}), and the number of ionizing photons per stellar atom (N_i):

$$f_\gamma = f_{esc} f_* N_i. \quad (1)$$

We allow f_γ to have different values, dependent on the mass of the halo, assuring it is consistent with reionization.

3. OUR MODELS

True first generation stars are metal free (Population III stars). As time goes on, stars die and enrich the universe, and eventually, these Population III stars give way to stars with metals (Population II stars). It is unclear when this happens, and this process is probably very inhomogeneous. Therefore, we assume two limiting cases - all of the stars from $6 < z < 30$ are either Population III ($Z = 0$) or Population II ($Z = 1/50 Z_\odot$) stars.

In addition to the metallicity, there is uncertainty for the mass spectrum of these stars. These stars could be very large, or they could be similar in size to what we see today. To model these two extremes, we choose either a heavy, Larson mass function (Larson 1998):

$$f(m) \propto m^{-1} \left(1 + \frac{m}{m_c}\right)^{-1.35}, \quad (2)$$

with mass limits of $m_1 = 3M_\odot$, $m_2 = 500M_\odot$, and $m_c = 250M_\odot$ to model a population of large stars, or a Salpeter mass function (Salpeter 1955):

$$f(m) \propto m^{-2.35}, \quad (3)$$

with mass limits of $m_1 = 3M_\odot$ and $m_2 = 150M_\odot$ to simulate a mass spectrum similar to what we see in the local universe.

If we combine our limiting cases for both mass and metallicity, we can establish our two limiting stellar models: Population III stars with a Larson mass spectra, and Population II stars with a Salpeter mass spectra. In reality, these stellar limits are extreme. In addition, we expect stellar properties to be inhomogeneous throughout redshift. However, these examples were chosen as limiting cases: which represent a population with the smallest and largest amplitude for the angular power spectrum of a large range of models, studied in detail in Fernandez et al. (2010). We would expect the actual amplitude for the angular power spectrum to lie between these extremes. These populations are summarized in Table 2.

4. COMPUTING THE FRACTIONAL ANISOTROPY

4.1. The Mean Cosmic Infrared Background

Now that we have our stellar and galactic models, we are in a position to calculate the fractional anisotropy, $\delta I/I$. To do this, we must compute both the mean intensity and the angular power spectrum of the CIB. The mean CIB is a combination of emission from the star, which is modeled as a stellar blackbody, and emission from the nebula, which is a combination of the Lyman- α line, two-photon, free-free and free-bound emission, and with the possibility of emission from dust (see section 4.2). This nebular emission is either produced within the halo itself, or within the IGM if some fraction of the ionizing radiation (f_{esc}) escapes the halo. However, the mean CIB does not depend on f_{esc} , since the nebular emission is the same, regardless of whether it is from the halo or the IGM.

Each emission process (stellar, free-free, free-bound, two-photon, and the Lyman- α) was modeled analytically (for details, see Fernandez & Komatsu (2006)) and integrated over a range of redshifts from $6 < z < 30$. The total intensity (I) is then:

$$I = \frac{c}{4\pi} \left(f_* \frac{\Omega_b}{\Omega_m}\right) \int \frac{dz}{H(z)(1+z)} \bar{\rho}_M^{halo}(z) \times [\bar{l}^*(z) + \bar{l}^{ff}(z) + \bar{l}^{fb}(z) + \bar{l}^{2\gamma}(z) + \bar{l}^{Ly\alpha}(z)]. \quad (4)$$

Here, $\bar{\rho}_M^{halo}(z)$ is the mean mass density collapsed into halos from the simulation. The luminosity per stellar mass, $\bar{l}(z)$, is given for each component of the luminosity, * for stellar, ff for free-free, fb for free-bound, 2γ for two-photon, and $Ly\alpha$ for Lyman-alpha emission. The luminosity of any component "α" can be written as¹:

$$l_\nu^\alpha(z) = \frac{d \ln \rho_*(z)}{dt} \frac{\int_{m_1}^{m_2} dm f(m) L_\nu^\alpha(m) \tau(m)}{\int_{m_1}^{m_2} dm f(m) m}. \quad (5)$$

The luminosity of each emission component (L_ν^α), and the stellar lifetime ($\tau(m)$) are integrated over a mass spectrum of stars. The first part of this expression is the inverse of the star formation time scale, $t_{SF}(z) =$

¹ This expression is only valid if the average stellar lifetime is always less than the star formation time scale t_{SF} , which is true for the cases we are concerned with. For more information, see Fernandez et al. (2010).

Simulation Name	Box Size (Mpc)	Minimum Halo Mass (M_\odot)	Suppression	$f_{\gamma,large}$	$f_{\gamma,small}$	z_{ov}	τ
Partial Suppression, High Efficiency	163	10^8	Yes	10	150	8.3	0.080
Partial Suppression, Low Efficiency	163	10^8	Yes	2	10	6.7	0.058
No Suppression	53	10^8	No	0.4	6	8.6	0.078
Complete Suppression	53	10^9	Yes - complete	12	0	8.3	0.071

TABLE 1

RADIATIVE TRANSFER SIMULATIONS USED IN THIS WORK. z_{ov} IS THE REDSHIFT OF OVERLAP, WHERE REIONIZATION IS COMPLETE, AND τ IS THE ELECTRON SCATTERING OPTICAL DEPTH. $f_{\gamma,small}$ IS FOR HALOS THAT ARE BETWEEN 10^8 AND $10^9 M_\odot$ WHILE $f_{\gamma,large}$ IS FOR HALOS ABOVE $10^9 M_\odot$.

f_γ	f_{esc}	f_* - Pop II Salpeter	f_* - Pop III Larson
10	0.1	3.8×10^{-2}	4.0×10^{-3}
10	0.3	1.3×10^{-2}	1.3×10^{-3}
10	0.5	7.7×10^{-3}	8.0×10^{-4}
10	1	3.8×10^{-3}	4.0×10^{-4}
150	0.1	5.8×10^{-1}	6.0×10^{-2}
150	0.3	1.9×10^{-1}	2.0×10^{-2}
150	0.5	1.2×10^{-1}	1.2×10^{-2}
150	1	5.8×10^{-2}	6.0×10^{-3}

TABLE 2

THE PROPERTIES OF THE STELLAR POPULATIONS. f_* WAS SET TO BE CONSISTENT WITH REIONIZATION.

$[\frac{d \ln \rho_*(z)}{dt}]^{-1}$. This star formation time scale is unknown, but we assume a value of 11.5 Myr, consistent with the value from simulations of Iliev et al. (2012). This expression then reduces to:

$$l_\nu^\alpha(z) = \frac{1}{t_{SF}(z)} \frac{\int_{m_1}^{m_2} dm f(m) L_\nu^\alpha(m) \tau(m)}{\int_{m_1}^{m_2} dm f(m) m} \quad (6)$$

(Fernandez et al. 2010).²

4.2. Dust

We do not know how much dust exists in high redshift galaxies. Molecular gas is already observed at $z \sim 5$, an indication that dust is present at those redshifts (Riechers et al. 2010). Because dust will affect the spectra of high redshift galaxies, the fractional anisotropy may also change. In order to see if our results are affected by dust, we compute the spectra expected if the radiation field is further reprocessed by a dusty medium. We generated a dust spectrum using DustEM (Compiègne et al. 2011) predicted for a galaxy with a high metallicity and minimal destruction of dust grains (Compiègne et al. 2010). In reality, the low metallicity and hard radiation fields expected at high redshift will lead to a dust contribution that is less than the one modeled here. In addition, DustEM models are computed in the optically thin limit, so therefore, the dusty SED we obtain is the upper limit for the amount that dust will redden. Our dusty model represents the extreme model for a dusty galaxy, with our case with no dust representing the opposing limit.

² The value chosen for t_{SF} will change the amplitude of the luminosity, which will both affect the mean and the fluctuations of the CIB. A benefit of taking the fractional anisotropy is that the dependence on t_{SF} will nearly cancel out. For more information on the dependence of the luminosity on t_{SF} , see section 6.1 of Fernandez et al. (2010).

4.3. Fluctuations in the Cosmic Infrared Background

The next step is to compute the angular power spectrum. These fluctuations will arise from both the emitting halos and their surrounding HII regions within the IGM. As shown in Fernandez et al. (2010), the fluctuations from the IGM are probably quite small (from 2 to 7 orders of magnitude smaller than that of the halos themselves) so can safely be ignored.

The angular power spectrum C_l can then be written as:

$$C_l = \frac{c}{(4\pi)^2} \left(f_* \frac{\Omega_b}{\Omega_m} \right)^2 \int \frac{dz}{H(z)r^2(z)(1+z)^4} \times [\bar{\rho}_M^{halo}(z) \{ \bar{l}^*(z) + (1 - f_{esc}) \bar{L}(z) \}]^2 \times b_{eff}^2 \left(k = \frac{l}{r(z)}, z \right) P_{lin} \left(k = \frac{l}{r(z)}, z \right). \quad (7)$$

Here b_{eff} is the effective bias, P_{lin} is the linear matter power spectra, $r(z) = c \int_0^z dz' / H(z')$ is the comoving distance, and the luminosity is:

$$\bar{L}(z) = \bar{l}^{ff}(z) + \bar{l}^{fb}(z) + \bar{l}^{2\gamma}(z) + \bar{l}^{Ly\alpha}(z). \quad (8)$$

The simulations provide both the halo bias and the linear matter density fluctuations. Note that the angular power spectrum depends on f_{esc} . The angular power spectrum of these simulations was computed in Fernandez et al. 2012.

4.4. The Fractional Anisotropy

The fractional anisotropy of the CIB is obtained by dividing the angular power spectrum C_l (shown in equation 7) by the mean intensity I (equation 4):

$$\delta I / I \equiv \sqrt{l(l+1)C_l / (2\pi I^2)}. \quad (9)$$

Most of the free parameters then cancel out, including the star formation efficiency f_* . The luminosity \bar{l}^α , however, will only cancel out when $f_{esc} = 0$. Therefore, the fractional anisotropy serves as a test to constrain f_{esc} .

5. RESULTS

At large values of l , the minimum mass of the star forming halos and suppression history will change the shape of the angular power spectrum due to non-linear bias effects (Fernandez et al. 2012). Since the minimum mass of these star forming halos is unknown, we compute the fractional anisotropy for $l = 3000$, avoiding any flattening or steepening of the angular power spectrum that could occur at larger l .

The fractional anisotropy at $l = 3000$ is shown in Figures 1 and 2 as a function of observed wavelength. The shaded regions are bounded by our two fiducial models (Population II stars with a Salpeter mass function will give the upper limit of the shaded region, while Population III stars with a Larson mass function will give the lower limit). Other reasonable models, varying the mass or metallicity of the stars, will lie between these two limiting cases, since the amplitude of the angular power spectrum will lie between these cases (Fernandez et al. 2010). We also show a range of f_{esc} , from $f_{esc} = 1$, (where all the ionizing photons escape from the halo into the IGM), to $f_{esc} = 0.1$. Results are shown for a case where reionization progresses with a high efficiency, the minimum halo mass is $10^8 M_\odot$, and small halos can be suppressed. However, these assumptions do not greatly affect the results.

As seen in this figure, the escape fraction has a large effect on $\delta I/I$. The mean level of the CIB, given in equation 4, has no dependence on the escape fraction. The angular power spectrum, given by equation 7, has a factor of $(1 - f_{esc})$. Therefore, when f_{esc} rises, the level of the nebular contribution to the angular power spectrum will fall. This causes the overall level of $\delta I/I$ to fall.

This drop-off of $\delta I/I$ for larger values of the escape fraction is more pronounced at longer wavelengths. To see why this occurs, we can look at the mean spectrum of starlight and nebular emission for a high redshift galaxy in Figure 3. (The definition of the bands shown are given in Table 3.) In the near-infrared bands ($\lambda < 4 \mu\text{m}$), there is always a large contribution from the stellar blackbody emission. At longer wavelengths, the stellar emission drops off very quickly, while, if the escape fraction is low, the nebular emission remains relatively high. If the escape fraction is high, however, the nebular emission component of the angular power spectrum would be diminished. This is particularly noticeable at longer wavelengths.

For small values of f_{esc} , the range of allowed values for $\delta I/I$ is quite narrow. This range widens if $f_{esc} = 1$. This is a consequence of the spectral shape for our two stellar models. For Population III stars, the blackbody spectrum of the star is steeper and there are more ionizing photons to be processed into nebular emission. The stellar spectrum is almost always equal to or less than that of the nebular component. On the other hand, the stellar blackbody is greater than the nebular component at short wavelengths for metal poor Population II stars. As the wavelength increases, the emission from the stellar component will drop below the level of emission from

Band	Central of Band (μm)	Waveband (μm)	$\Delta\lambda/\lambda$
J	1.25	1.1 - 1.4	24%
H	1.65	1.5 - 1.8	18%
K	2.2	2.0 - 2.4	18%
L	3.5	3.0 - 4.0	29%
M	4.8	4.6 - 5.0	8.3%
N	11	7.5 - 14.5	64%
Q	21	17 - 25	38%
Z	34	28 - 40	35%
H1	75	60 - 90	40%
H2	110	90 - 130	36%
H3	170	130 - 210	47%

TABLE 3
BAND DEFINITIONS USED FOR INFRARED BANDS. H1, H2, AND H3 DENOTE THE BANDS OF THE HERSCHEL PACS INSTRUMENT. ALL BANDS ARE ASSUMED TO BE RECTANGULAR.

the nebula. If f_{esc} is small, the total emission of the halos for Population III and Population II stars is similar, so the range of $\delta I/I$ is narrow. If f_{esc} is large, the amplitude of the angular power spectrum of large Population III stars will be more affected than smaller Population II stars, widening the range of allowed values of $\delta I/I$.

In Figure 2, we see the the fractional anisotropy for the case when galaxies contain dust. Here, we no longer see a decrease in $\delta I/I$ at long wavelengths. This is because dust will reprocess the stellar and nebular emission, re-emitting the light at longer wavelengths. (An illustration of the SED with dust included is also shown in Figure 3.) Unlike nebular emission, the dust component will not fall to zero when $f_{esc} = 1$. In fact, the change between the dust emission from $f_{esc} = 0$ and $f_{esc} = 1$ is only slight. Therefore, while the nebular component will disappear if $f_{esc} = 1$, the dust component will still be present, causing the angular power spectrum at long wavelengths to remain high, raising $\delta I/I$. This is a direct result from the fact that nebular emission only results from ionizing photons, while photons of lower energies can be converted into dust emission.

6. COMPARISON TO OBSERVATIONS

Measurements of the CIB are notoriously hard to perform. Finding an accurate mean is particularly difficult because precise foreground subtraction is needed. However, observations, such as with CIBER, AKARI, and Herschel, continue to improve, resolving foregrounds in more detail and obtaining more reliable observations for the CIB.

Many observations have been made to try to understand the contribution of high redshifts to the CIB from 1-4 microns. In order to uncover any residual emission in the mean or fluctuation observations, one must carefully take into account all of the foreground components. Zodiacal light is a major contaminant, and because it is very difficult to model, it is not straightforward to subtract from the CIB. In addition, foreground galaxies at lower redshifts must be taken into account. Despite the difficulty, there have been many attempts to measure the mean level of the CIB in the near-infrared due to high redshift stars (Dwek & Arendt 1998; Gorjian et al. 2000; Kashlinsky & Odenwald 2000; Wright & Reese 2000; Wright 2001; Cambr esy et al. 2001; Totani et al. 2001; Kashlinsky et al. 2002, 2004; Kashlinsky 2005; Kashlinsky et al. 2007a,b, 2012; Magliocchetti et al.

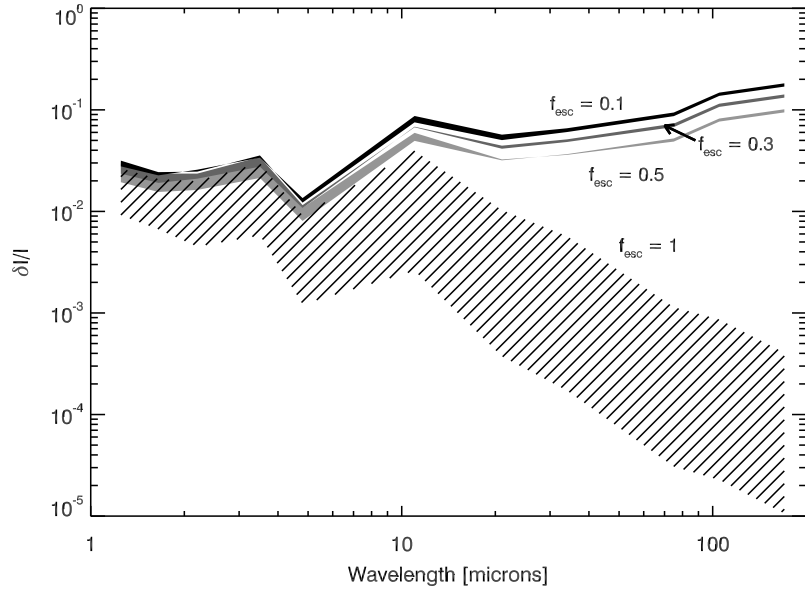


FIG. 1.— The Fractional Anisotropy, $\delta I/I$, as a function of wavelength, for various values of f_{esc} , in cases without dust. Population II stars with a Salpeter mass spectrum provide the upper limit of the shaded regions, while Population III stars with a Larson mass spectrum provide the lower limits. Other reasonable assumptions for the mass and metallicity of the stellar populations should lie within the shaded regions.

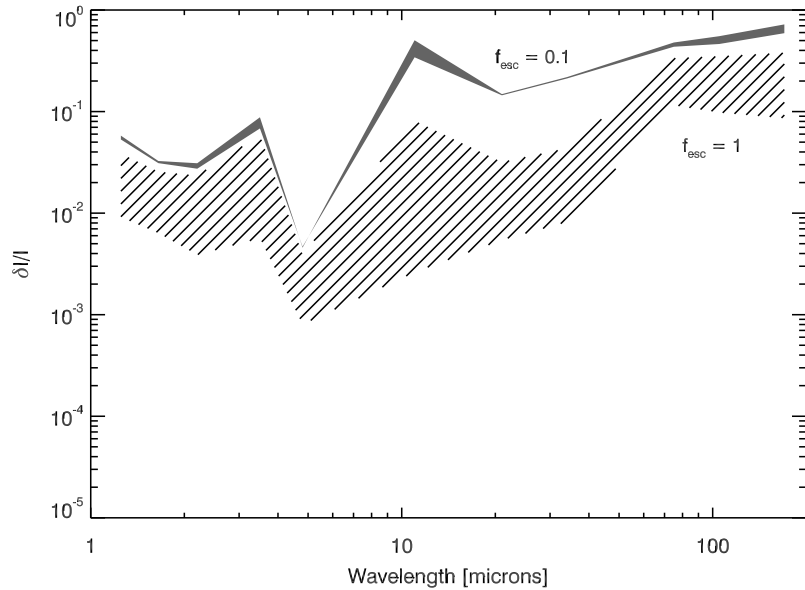


FIG. 2.— The Fractional Anisotropy, $\delta I/I$, as a function of wavelength, for cases with dust.

2003; Odenwald et al. 2003; Cooray et al. 2004; Matsumoto et al. 2005; Thompson et al. 2007a,b).

Fluctuation observations are, in theory, easier to perform, since they do not need an accurate zero point, and instead rely on variations from one region of the sky to another. However, these observations still rely on careful and complete subtraction of foreground sources, and also remain controversial (Kashlinsky et al. 2005, 2007b, 2012; Cooray et al. 2007; Thompson et al. 2007a; Matsumoto et al. 2011).

Observations are even more difficult in the mid and

far-infrared. One problem is that foregrounds that were present in the near-infrared are even more prevalent in the mid and far-infrared. Zodiacal light peaks at about $20 \mu m$, which washes out most detections of the CIB in this range. In addition, Galactic cirrus is a main contaminant, however, observations are possible in clean regions of the sky. Finally, as wavelength increases, foreground galaxies become more difficult to resolve. All of these problems lead to only a fraction of the CIB in the mid and far-infrared being resolved into low-redshift galaxies. It is likely that only a very small (and currently

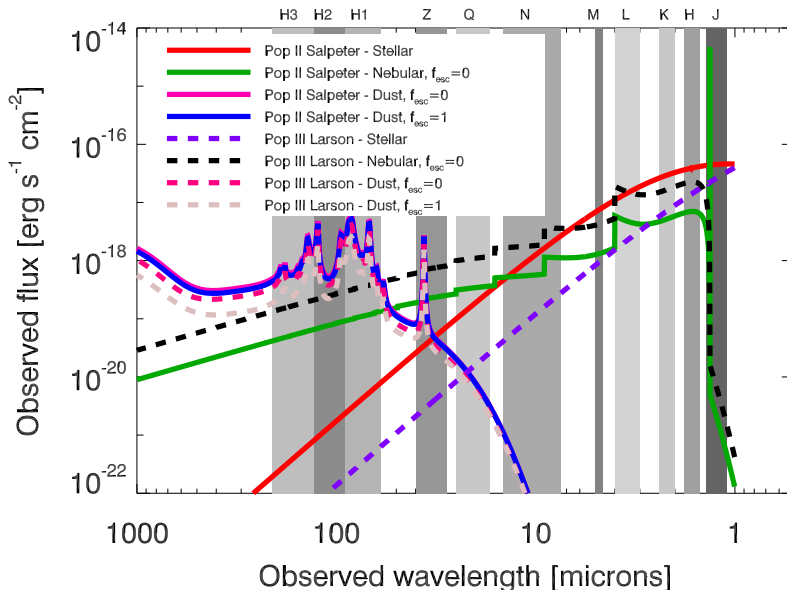


FIG. 3.— The spectra of a $10^9 M_{\odot}$ galaxy at $z = 10$. We assume a star formation efficiency of $f_* = 0.1$. Two stellar populations are shown - Population II stars with a Salpeter mass spectrum, or Population III stars with a Larson mass spectrum. In addition, two limiting cases of the escape fraction are shown - $f_{esc} = 0$ and $f_{esc} = 1$. When $f_{esc} = 0$, the ionizing radiation stays within the galaxy, creating nebular emission, which is not present in the halo if $f_{esc} = 1$. The dust emission will fall only slightly when $f_{esc} = 1$. Bands are denoted by the shaded gray regions. Herschel PACS bands are labeled as H1, H2, and H3.

unknown) percentage of this excess is from $z > 6$, so care must be taken in interpreting observations.

There has been a great push to understand the CIB at longer wavelengths. At 100 and 160 μm , Pénin et al. (2011) measured the mean and fluctuation power of galaxies at all redshifts using observations from IRIS/IRAS and Spitzer/MIPS, respectively. Fluctuations of the cumulative CIB have been taken in the mid-infrared to submillimeter wavelengths (Kashlinsky & Odenwald 2000; Lagache & Puget 2000; Miville-Deschênes et al. 2002; Grossan & Smoot 2007; Lagache et al. 2007; Amblard et al. 2011; Matsuura et al. 2011; Planck Collaboration et al. 2011; Pyo et al. 2012). The cumulative mean level of the CIB from galaxies at all redshifts has been measured as well (Fixsen et al. 1998; Hauser et al. 1998; Lagache et al. 2000; Wright 2004; Odegard et al. 2007; Matsuura et al. 2011). The mean CIB has been measured as a function of redshift (Berta et al. 2011; Jauzac et al. 2011; Béthermin et al. 2012), while measurements from BLAST and *Planck* from 250 to 1400 microns (Planck Collaboration et al. 2011) could indicate that galaxies at a higher redshift (here, $z > 1.2 - 2$) could contribute more to the CIB as the wavelength increases. Currently, the best measurements (Planck Collaboration et al. 2011; Viero et al. 2009) show that the fractional anisotropy is at the order of 15%, however, these measurements include galaxies at all redshifts.

One way to subtract unresolved low redshift galaxies in the mid to far-infrared to a more complete level is to use a stacking algorithm. This typically involves using the locations of known galaxies at a shorter wavelength, stacking these locations of a longer wavelength image, and utilizing this stack to calculate the CIB ac-

counted from these galaxies. If stacking is relied upon, more of the CIB at long wavelengths can be resolved into lower redshift galaxies. For example, Marsden et al. (2009) used stacking to resolve 100% of the CIB as detected with FIRAS (Fixsen et al. 1998) at 250, 350, and 500 microns using BLAST. Dole et al. (2006) used 24 μm sources from Spitzer/MIPS data to stack images at 70 and 160 μm . They were able to resolve 79%, 92 %, and 69% of the CIB at 24, 70, and 160 μm respectively. Berta et al. (2010) resolved 45% and 52% (without stacking) and 50% and 75% (with stacking) of the CIB at 100 and 160 μm using Herschel/PACS data. At longer wavelengths, Greve et al. (2010) resolved 16.5% of the CIB at 870 microns using stacking. While it is possible that some of the remaining flux is from low redshift galaxies, it is also possible that some of this unresolved CIB could be due to high redshift galaxies. (See, for example, Matsuura et al. (2011)).

We compare some of these observations to our models for the fractional anisotropy at high redshifts. While precise measurements of the mean are challenging, measurements of the fluctuation power are becoming more reliable. Because of this, in Figure 4 we show the fractional anisotropy predicted using various recent observations of the fluctuation power, assuming an upper limit of the mean CIB due to high redshift stars is either 10 $\text{nW m}^{-2} \text{sr}^{-1}$ or 1 $\text{nW m}^{-2} \text{sr}^{-1}$. Because it is unlikely that a $z > 6$ component of the mean CIB will be much higher than this, very low values of $\delta I/I$, and thus very high values of the escape fraction from a dust-free population, can be ruled out. More definitive conclusions can be reached as observations continue to improve and our understanding of foreground emission grows.

It is important to remember that there is still low-redshift contamination contributing to both the

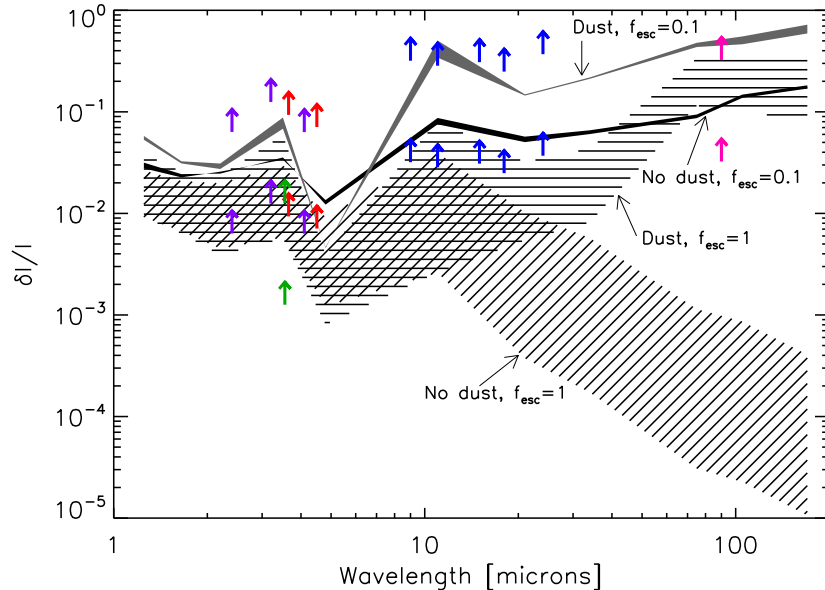


FIG. 4.— The Fractional Anisotropy, $\delta I/I$, in comparison to recent observations. The upper limit of the mean CIB from $z > 6$ stars is assumed to be either $10 \text{ nW m}^{-2} \text{ sr}^{-1}$ (lower set of arrows) or $1 \text{ nW m}^{-2} \text{ sr}^{-1}$ (upper set of arrows). These assumptions provide the lower limits of $\delta I/I$. Shown are observations from Kashlinsky et al (2012) (red arrows), Matsumoto et al (2011) (purple arrows), Cooray et al (2007) (green arrows), Pyo et al (2012) (blue arrows), and Matsuura et al (2011) (pink arrows). The horizontal hatched region shows cases with dust and $f_{esc} = 1$, the diagonal hatched region shows cases with no dust and $f_{esc} = 1$, the grey shaded region shows cases with dust and $f_{esc} = 0.1$, and the black region shows cases with no dust and $f_{esc} = 0.1$.

mean and fluctuations, especially at longer wavelengths. Therefore, these results should be interpreted with this in mind. As observations improve, these results will become more reliable.

7. CONCLUSIONS

We have shown the observable signatures of high redshift populations with different values of the escape fraction f_{esc} and dust content in the CIB. It is possible to distinguish these populations through observations of the fractional anisotropy of the CIB. The global escape fraction of high redshift galaxies is a main variable that can be probed in this way, since the angular power spectrum is dependent on it, while the mean is not. In addition, dust will transform the SED of the galaxy, thus leaving an imprint on the fractional anisotropy. Therefore, low values of the fractional anisotropy will be indicative of a population of stars with a high escape fraction and little dust. This will be more noticeable at

longer wavelengths. While observations are still difficult, improved observations could be able to distinguish between these populations.

We would like to thank Masami Ouchi and Kristian Finlator for helpful discussions. In addition, we would like to thank Melanie Koehler and Laurent Verstraete for help with DustEM. This work was supported by the Science and Technology Facilities Council [grant numbers ST/F002858/1 and ST/I000976/1]; the ANR program ANR-09-BLAN-0224-02, and The Southeast Physics Network (SEPNet). The authors acknowledge the Texas Advanced Computing Center (TACC) at The University of Texas at Austin for providing HPC resources that have contributed to the research results reported within this paper. URL: <http://www.tacc.utexas.edu>. This research was supported in part by the National Science Foundation through TeraGrid resources provided by TACC and NICS.

REFERENCES

- Amblard, A., et al. 2011, *Nature*, 470, 510
 Berta, S., et al. 2010, *A&A*, 518, L30+
 —. 2011, *A&A*, 532, 49
 Béthermin, M., et al. 2012, *A&A*, 542, A58
 Bouwens, R. J., et al. 2010, *ApJL*, 708, L69
 Cambrésy, L., Reach, W. T., Beichman, C. A., & Jarrett, T. H. 2001, *ApJ*, 555, 563
 Compiègne, M., Flagey, N., Noriega-Crespo, A., Martin, P. G., Bernard, J.-P., Paladini, R., & Molinari, S. 2010, *ApJL*, 724, L44
 Compiègne, M., et al. 2011, *A&A*, 525, A103
 Cooray, A., Bock, J. J., Keatin, B., Lange, A. E., & Matsumoto, T. 2004, *ApJ*, 606, 611
 Cooray, A., & Yoshida, N. 2004, *MNRAS*, 351, L71
 Cooray, A., et al. 2007, *ApJL*, 659, L91
 Dole, H., et al. 2006, *A&A*, 451, 417
 Dwek, E., & Arendt, R. G. 1998, *ApJL*, 508, L9
 Fernandez, E. R., Iliev, I. T., Komatsu, E., & Shapiro, P. R. 2012, *ApJ*, 750, 20
 Fernandez, E. R., & Komatsu, E. 2006, *ApJ*, 646, 703
 Fernandez, E. R., Komatsu, E., Iliev, I. T., & Shapiro, P. R. 2010, *ApJ*, 710, 1089
 Fernandez, E. R., & Shull, J. M. 2011, *ApJ*, 731, 20
 Fixsen, D. J., Dwek, E., Mather, J. C., Bennett, C. L., & Shafer, R. A. 1998, *ApJ*, 508, 123
 Gorjian, V., Wright, E. L., & Chary, R. R. 2000, *ApJ*, 536, 550
 Greve, T. R., et al. 2010, *ApJ*, 719, 483
 Grossan, B., & Smoot, G. F. 2007, *A&A*, 474, 731
 Hauser, M. G., et al. 1998, *ApJ*, 508, 25
 Iliev, I. T., Mellema, G., Shapiro, P. R., Pen, U.-L., Mao, Y., Koda, J., & Ahn, K. 2012, *MNRAS*, 423, 2222
 Jauzac, M., et al. 2011, *A&A*, 525, A52+

- Kashlinsky, A. 2005, *Phys. Rep.*, 409, 361
- Kashlinsky, A., Arendt, R., Gardner, J. P., Mather, J. C., & Moseley, S. H. 2004, *ApJ*, 608, 1
- Kashlinsky, A., Arendt, R. G., Ashby, M. L. N., Fazio, G. G., Mather, J., & Moseley, S. H. 2012, *ApJ*, 753, 63
- Kashlinsky, A., Arendt, R. G., Mather, J., & Moseley, S. H. 2005, *Nature*, 438, 45
- . 2007a, *ApJL*, 666, L1
- . 2007b, *ApJL*, 654, L5
- . 2007c, *ApJL*, 654, L1
- Kashlinsky, A., & Odenwald, S. 2000, *ApJ*, 528, 74
- Kashlinsky, A., Odenwald, S., Mather, J., Skrutskie, M. F., & Cutri, R. M. 2002, *ApJL*, 579, L53
- Komatsu, E., et al. 2009, *ApJS*, 180, 330
- . 2011, *ApJS*, 192, 18
- Lagache, G., Bavouzet, N., Fernandez-Conde, N., Ponthieu, N., Rodet, T., Dole, H., Miville-Deschênes, M.-A., & Puget, J.-L. 2007, *ApJL*, 665, L89
- Lagache, G., & Puget, J. L. 2000, *A&A*, 355, 17
- Lagache, G., et al. 2000, in *Lecture Notes in Physics*, Berlin Springer Verlag, Vol. 548, *ISO Survey of a Dusty Universe*, ed. D. Lemke, M. Stickel, & K. Wilke, 81–+
- Larson, R. B. 1998, *MNRAS*, 301, 569
- Madau, P., & Silk, J. 2005, *MNRAS*, 359, L37
- Magliocchetti, M., Salvaterra, R., & Ferrara, A. 2003, *MNRAS*, 342, L25
- Marsden, G., et al. 2009, *ApJ*, 707, 1729
- Matsumoto, T., et al. 2005, *ApJ*, 626, 31
- . 2011, *ApJ*, 742, 124
- Matsuura, S., et al. 2011, *ApJ*, 737, 2
- Miville-Deschênes, M.-A., Lagache, G., & Puget, J.-L. 2002, *A&A*, 393, 749
- Odegard, N., Arendt, R. G., Dwek, E., Haffner, L. M., Hauser, M. G., & Reynolds, R. J. 2007, *ApJ*, 667, 11
- Odenwald, S., Kashlinsky, A., Mather, J. C., Skrutskie, M. F., & Cutri, R. M. 2003, *ApJ*, 583, 535
- Pénin, A., et al. 2011, *A&A*, 543, 123
- Planck Collaboration et al. 2011, *A&A*, 536, A18
- Pyo, J., Matsumoto, T., Jeong, W.-S., & Matsuura, S. 2012, *ArXiv* 1202.4049
- Riechers, D. A., et al. 2010, *ApJL*, 720, L131
- Robertson, B. E., Ellis, R. S., Dunlop, J. S., McLure, R. J., & Stark, D. P. 2010, *Nature*, 468, 49
- Salpeter, E. E. 1955, *ApJ*, 121, 161
- Salvaterra, R., & Ferrara, A. 2003, *MNRAS*, 339, 973
- Santos, M. R., Bromm, V., & Kamionkowski, M. 2002, *MNRAS*, 336, 1082
- Thompson, R. I., Eisenstein, D., Fan, X., Rieke, M., & Kennicutt, R. C. 2007a, *ApJ*, 657, 669
- . 2007b, *ApJ*, 666, 658
- Totani, T., Yoshii, Y., Iwamuro, F., Maihara, T., & Motohara, K. 2001, *ApJL*, 550, L137
- Viero, M. P., et al. 2009, *ApJ*, 707, 1766
- Wright, E. L. 2001, *ApJ*, 553, 538
- . 2004, *New AR*, 48, 465
- Wright, E. L., & Reese, E. D. 2000, *ApJ*, 545, 43